PAPER

Check for updates

Synthesis of thermoresponsive PNIPAm-*b*-PVP-*b*-PNIPAm hydrogels *via* aqueous RAFT polymerization†

Lauren E. Ball, [ID] ‡ Gabriela Garbonova,‡ Rueben Pfukwa [ID] * and Bert Klumperman [ID] *

Stimuli-responsive BAB type triblock copolymers of poly(*N*-isopropyl acrylamide) and poly(*N*-vinylpyrrolidone) *i.e.* PNIPAm-*b*-PVP-*b*-PNIPAm were readily synthesized *via* aqueous reversible addition–fragmentation chain transfer (RAFT) mediated polymerization using a difunctional xanthate RAFT agent, with redox initiation, under mild conditions. The thermoresponsive behavior and temperature-induced self-assembly in aqueous media was studied using turbidimetry, variable temperature dynamic light scattering (VT DLS), VT ^{1}H NMR spectroscopy and transmission electron microscopy. With increasing temperature, above the critical solution temperature of the PNIPAm segments, the triblock copolymers self-assemble into flower-like micelles with a PNIPAm core. Concentrated aqueous solutions (>20 wt%) displayed a thermo-reversible sol–gel transition, as shown by test-tube inversion and injectability tests. Thermogellation was further confirmed *via* variable temperature rheology. This study establishes the potential for PNIPAm-*b*-PVP-*b*-PNIPAm systems to be incorporated in biomedical research as potential drug delivery devices *via* injectable hydrogel systems.

Introduction

Polymeric hydrogels are three-dimensional hydrophilic network structures that can form materials with soft physical properties analogous to soft tissue, upon imbibing large volumes of water.[1–3] Most synthetic hydrogels are highly biocompatible materials and, due to their soft and hydrophilic nature, have important biomedical applications, for example as scaffolds for tissue engineering, as implants and as drug delivery systems.[4–6] These gels can either be chemically or physically crosslinked.[7,8] Chemically crosslinked hydrogels often requires low molecular weight crosslinking agents which may be harmful for *in vivo* applications.[5] Contrarily, physical hydrogels are held together by noncovalent interactions between soluble building blocks. Of these, smart polymeric hydrogels with *in situ* sol–gel transition capabilities triggered by stimuli (*e.g.*, temperature) under normal physiological conditions, have appealing biomedical applications including controlled drug delivery and regenerative tissue engineering.[5,7,9,10] A prominent class of these hydrogels is based on thermo-

responsive polymers incorporated as the outer blocks of an ABA triblock copolymer (tBCP) with a permanent hydrophilic central block. Aqueous solutions of these tBCPs gel at physiological temperatures due to self-assembly driven by the responsive blocks.[11–13] Heating aqueous solutions of such tBCPs leads to the collapse of the thermoresponsive blocks which self-assemble into flower-like micelles when in dilute solutions. Upon an increase in concentration, *i.e.*, above the critical gelation concentration (CGC), a 3-dimensional micellar network layer is formed, in which the central hydrophilic block forms bridges with neighboring micelles.[13,14] Consequently, the free-flowing solution is transformed into a free-standing micellar hydrogel triggered by changes in the environmental temperature. Physiological temperatures are always set in the range of 35–37 °C, regardless of organ/tissue/cell, unlike ionic and pH levels, which fluctuate depending on the target site.[15] This makes temperature the most interesting trigger mechanism for controlled drug delivery systems, as no consideration to a specific target site is necessary.

Poly(*N*-isopropyl acrylamide) (PNIPAm) is the most widely studied thermoresponsive polymer as it undergoes a coil-to-globule transition in aqueous solution upon reaching its lower critical solution temperature (LCST) of around 32 °C, close to physiological conditions.[16–18] It has been combined, in varying architectures, with polyethylene oxide,[19] poly(2-ethyl-2-oxazoline) (PEOx),[20] poly(*N*,*N*-dimethylacrylamide) (PDMA),[21] and

Department of Chemistry and Polymer Science, Stellenbosch University, Private Bag X1, Matieland 7602, South Africa. E-mail: rueben@sun.ac.za, bklump@sun.ac.za

‡Both authors contributed equally to this manuscript.

poly(acrylic acid) and its derivatives,[22–24] amongst others, to form thermoresponsive tBCP gels. The desired ABA/BAB tBCPs are accessed in a variety of ways, *i.e.*, using bifunctional ATRP initiators,[14] or RAFT chain transfer agents,[25–28] and consecutive monomer addition approaches.[29] Where different combinations of polymer classes are used, a crossover in polymerization methods is necessary. For example, with the PNIPAm-*b*-PEOx-*b*-PNIPAm (BAB-type) triblocks reported by Sahn *et al.* the A block, prepared *via* cationic ring opening polymerization, was end-capped with RAFT chain transfer agents enabling a crossover to PNIPAm synthesis *via* a reversible deactivation radical polymerization process.[20]

A challenge with reported synthetic procedures for making these tBCPs, is the use of organic solvents which are often uneconomical, toxic, and environmentally unfriendly.[30] This can be improved by judicious choice of polymer combinations and polymerization methods. Poly(*N*-vinylpyrrolidone) (PVP) is a water-soluble, biocompatible, non-ionic and (relatively) chemically inert polymer. For these reasons it finds use in the pharmaceutical industry as a drug excipient, in cosmetics, adhesives, coatings and inks.[31–35] Polymer hydrogels incorporating PVP have found use as stimuli responsive drug delivery systems,[36] and as scaffolds for bone tissue engineering where the unique hydrophilic/hydrophobic balance that PVP provides aids bone regeneration.[37] It can be envisaged that the copolymer of PNIPAm/PVP is a potentially interesting candidate for fabricating biocompatible hydrogels with potential application as stimuli responsive drug delivery materials. Both PNIPAm and PVP are readily obtained *via* the RAFT polymerization process, in aqueous media, at ambient conditions.[38,39] By using a bifunctional xanthate RAFT agent capable of mediating the synthesis of PNIPAm and PVP, an appealing straightforward approach for tBCPs with a BAB architecture, in water, was envisaged, Scheme 1. This approach allows one to combine two polymer types using a single polymerization technique, in water, whilst avoiding post-polymerization functionalization, which would lengthen the synthetic method.
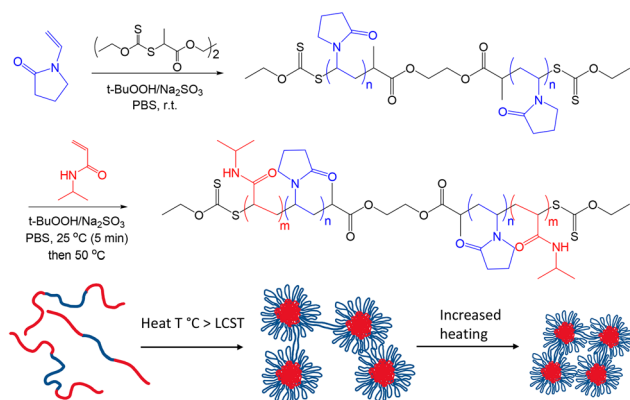
In this work, well-defined BAB-type tBCPs of PNIPAm-*b*-PVP-*b*-PNIPAm are synthesized *via* aqueous RAFT-mediated polymerization process using a symmetrical difunctional xanthate-based RAFT agent, first preparing a PVP A-block before chain extending with PNIPAm B-blocks. To the best of our knowledge, there are no reported examples of this tBCP system being synthesized without the use of organic solvents. We then investigate the temperature-responsive properties of the triblock copolymers and study the effect of copolymer composition, concentration, and molecular weight on gelation.

Experimental

Materials and methods

All chemicals and solvents were purchased from commercial sources and used without further purification, unless otherwise stated. Oxygen sensitive reactions were carried out under inert atmosphere using argon gas. All compounds were characterized by ^{1}H and ^{13}C NMR spectroscopy using a Varian VXR-Unity (300 MHz, 400 MHz or 600 MHz) spectrometer. Samples were prepared in deuterated solvents, CDCl$_3$ and D$_2$O, and chemical shifts were reported in parts per million (ppm), where the residual solvent peaks were used as internal reference. Variable temperature (VT) ^{1}H NMR spectra were recorded on samples dissolved in D$_2$O at a concentration of 15 mg mL^{-1}. The samples were analysed in temperature steps of 2 °C starting from 20 °C to 60 °C. At each temperature step, the samples were equilibrated before the measurement was taken.

Synthesis of RAFT agent

The difunctional xanthate chain transfer agent was synthesized according to reported procedures (yield of 60%),[40] and RAFT agent purity was assessed *via* ^{1}H NMR spectroscopy (91%). ^{1}H NMR (600 MHz, CDCl$_3$): δ 4.64 (q, 4H, (CH$_3$–C**H$_2$**–O–(C=S)–S–CH–CH$_3$–O–CH$_2$–)$_2$), 4.44–4.31 (m, 7H, (CH$_3$–CH$_2$–O–(C=S)–S–C**H**–CH$_3$–O–C**H$_2$**–)$_2$), 1.58 (d, 6H, (CH$_3$–CH$_2$–O–(C=S)–S–CH–C**H$_3$**–O–CH$_2$–)$_2$, 1.42 (t, 6H, (C**H$_3$**–CH$_2$–O–(C=S)–S–CH–CH$_3$–O–CH$_2$–)$_2$.

Synthesis of PVP macro-CTA

A library of PVP macro-CTAs was synthesised *via* RAFT mediated polymerization, with varying molecular weight targets as summarised in Table 1 and Table S1.† PVP$_{179}$ (Table S1†) was synthesised according to the following

Scheme 1 Synthesis of PNIPAm-*b*-PVP-*b*-PNIPAm triblock copolymers *via* RAFT mediated polymerization. Self-assembly of a tBCP in concentrated aqueous solution, from unimers to networked flower-like micelles, as well as shrinkage and formation of additional crosslinks.

Table 1 RAFT mediated polymerization of NVP

Sample	M_n^{target} (g mol^{-1})	α^a (%)	$M_n^{theo\ b}$ (g mol^{-1})	$M_n^{NMR\ c}$ (g mol^{-1})	$M_n^{SEC\ d}$ (g mol^{-1})	$Đ^d$
PVP$_{100}$	17 000	70	12 400	10 000	12 000	1.30
PVP$_{160}$	30 000	60	18 400	20 400	18 500	1.20

^{a} Conversion determined gravimetrically. ^{b} Calculated using α. ^{c} Determined *via* ^{1}H NMR spectroscopy. ^{d} Determined *via* SEC using DMF as the mobile phase (0.05 M LiBr) and PMMA calibration standards.

method, as a representative example. NVP (4.5 g, 40 mmol), xanthate (0.067 g, 0.16 mmol), tBuOOH (0.0014 g, 0.016 mmol) and PBS (pH 7.4, 2.3 mL) were added to a round bottom flask fitted with a bubbler and rubber septum and the mixture sparged with dry argon for 30 min. Na_2SO_3 (0.0020 g, 0.016 mmol) in PBS (1 mL) was sparged with argon separately and after 30 min added to the reaction mixture using a degassed syringe and the reaction mixture sparged with argon for an additional 5 min and then allowed to stir at ambient temperature for 16 h. The reaction mixture was then transferred into a 3500 MWCO dialysis tubing, dialysed in water for two days, with water changes occurring 2–3 times per day, and subsequently lyophilised.

Synthesis of PNIPAm-*b*-PVP-*b*-PNIPAm

A library of PNIPAm-*b*-PVP-*b*-PNIPAm was synthesised *via* RAFT mediated polymerization, with varying molecular weight targets as summarised in Table 2 and Table S2.† $PNIPAm_{234}$-*b*-PVP_{179}-*b*-$PNIPAm_{234}$ (A_{179}–$(B_{234})_2$ in Table S2†) was synthesised according to the following method as a representative example. PVP_{179} (0.69 g, 0.034 mmol), NIPAm (1.8 g, 16 mmol), tBuOOH (0.6 mg, 7 μmol) and PBS (pH 7.4, 15.8 mL) were added to a round bottom flask fitted with a bubbler and rubber septum and the mixture sparged with dry argon for 30 min. Na_2SO_3 (0.9 mg, 7 μmol) in 1 mL PBS was sparged with dry argon separately and added to the reaction mixture using a degassed syringe after 30 min. The reaction mixture was sparged with argon for an additional 5 min and depending on the chain extension experiment, the temperature and duration of the polymerization was varied and is specified per sample. The reaction was quenched *via* exposure to atmospheric oxygen and the reaction mixture transferred to 3500 MWCO dialysis tubing and the sample dialysed in water for two days, with water changes occurring 2–3 times per day, before lyophilisation. Kinetic experiments were conducted using a similar procedure, where reaction temperature and initiator concentration were varied, with sampling intervals specified for each individual experiment (Table S2, Fig. S4–S10†). tBCP libraries were synthesised using the above procedure, where initiator was added and the reaction mixture

stirred at ambient temperature before being heated to 50 °C (Table 2).

Size exclusion chromatography (SEC)

SEC analyses was conducted on a system equipped with a Shimadzu LC-10AT isocratic pump, a Waters 717+ autosampler, a column system fitted with a PSS guard column (50 × 8 mm) in series with three PSS GRAM columns (300 × 8 mm, 10 μm, 2 × 3000 Å and 1 × 100 Å) maintained at 40 °C, a Waters 2414 differential refractive index (DRI) detector and a Waters 2487 dual wavelength UV detector. Dimethylformamide (DMF) was used as eluent, stabilized with 0.05 M LiBr, at a flow rate of 1.0 mL min^{-1}. Polymer samples were filtered through 0.45 μm PTFE filters prior to analysis. The molar masses were calculated against poly(methyl methacrylate) (PMMA) standards (Polymer Laboratories) ranging from 690 to $1.2 × 10^6$ g mol^{-1}. SEC data was processed using Millenium software (version 4).

Turbidimetry

Turbidity measurements were performed on a PerkinElmer Lamda 20 photodiode array spectrophotometer, consisting of a holographic monochromator pre-aligned deuterium and halogen lamps and a photodiode array detector. A temperature controller was connected, and measurements of the temperature were taken. The sample concentrations ranged from 5–25 wt%. The transmittance at 500 nm was monitored, with temperature ramped from 20 °C to 80 °C and back, with 2 °C increments and an equilibration time of 5 minutes before each measurement. The cloud point temperature (T_{CP}) was set as the maximum of the first derivative of the transmittance data. Three independent measurements were performed for each sample.

Dynamic light scattering (DLS)

DLS was performed on a ZetaSizer 1000 HSa (Malvern Instruments, Malvern) equipped with a 4 mW He–Ne laser, operating at a wavelength of 633.0 nm and a scattering angle of 90°. The sample concentrations were kept constant at 1 mg mL^{-1}. Samples were heated from 20 °C to 50 °C in 2 °C steps.

Table 2 RAFT mediated chain extension of PVP macro-CTA with PNIPAm

Sample	M_n^{target} (g mol^{-1})	α^a	$M_n^{SEC\ b}$ (g mol^{-1})	$Đ^b$	Copolymer composition^c	PNIPAm : PVP^d	f_{PVP}^e (%)
tBCP1-A	26 000	98	34 000	1.30	PNIPAm$_{70}$-*b*-PVP$_{160}$-*b*-PNIPAm$_{70}$	39 : 61	53
tBCP1-B	33 000	100	44 000	1.34	PNIPAm$_{115}$-*b*-PVP$_{160}$-*b*-PNIPAm$_{115}$	55 : 45	41
tBCP1-C	36 000	100	45 000	1.35	PNIPAm$_{120}$-*b*-PVP$_{160}$-*b*-PNIPAm$_{120}$	59 : 41	40
tBCP1-D	48 000	100	66 000	1.34	PNIPAm$_{210}$-*b*-PVP$_{160}$-*b*-PNIPAm$_{210}$	70 : 30	28
tBCP2-A	17 000	97	25 000	1.31	PNIPAm$_{57}$-*b*-PVP$_{100}$-*b*-PNIPAm$_{57}$	35 : 65	48
tBCP2-B	20 000	97	30 000	1.30	PNIPAm$_{80}$-*b*-PVP$_{100}$-*b*-PNIPAm$_{80}$	48 : 52	40
tBCP2-C	24 000	97	38 000	1.26	PNIPAm$_{115}$-*b*-PVP$_{100}$-*b*-PNIPAm$_{115}$	58 : 42	32
tBCP2-D	30 000	96	53 000	1.24	PNIPAm$_{180}$-*b*-PVP$_{100}$-*b*-PNIPAm$_{180}$	70 : 30	24

All chain extensions conducted using [PVP macro-CTA] : [I] of 1 : 0.2, at 15 wt% in PBS, where the polymerization is allowed to proceed at 25 °C for 5 min, then 50 °C for 5 h. ^{a} Conversion determined gravimetrically. ^{b} Determined *via* SEC with DMF as the mobile phase (0.05 M LiBr) and PMMA calibration standards. ^{c} PNIPAm-*b*-PVP-*b*-PNIPAm composition determined using M_n^{SEC} of homopolymer and triblock copolymer. ^{d} Ratios calculated *via* ^{1}H NMR analysis using integrated signals of PNIPAm and combined signals of PNIPAm and PVP. ^{e} Calculated using M_n^{SEC} (M_n homo/M_n triblock × 100).

The samples were equilibrated for 300 s at each temperature step and measured three times. Each measurement comprised of 10–15 sub-runs to determine the particle sizes. The volume distribution of the particle size was then calculated using CONTIN analysis.

Sol–gel test tube inversion study

Sol–gel phase transition was determined by using the test-tube inversion method. The transition was monitored visually by inverting the test tubes. The criteria for a sol or gel were defined as "flowing" or "non-flowing" for one minute, respectively. Samples were prepared at different concentrations, from 5 to 25 wt%, in 1 mL volumes of deionized water. The samples were placed in a water bath and heated from 20 °C to 60 °C at a rate of 0.5 °C min⁻¹ after which the samples were removed and immediately tested for gelation.

Rheology

Rheology measurements were carried out on an Anton Paar Physica MCR501 using parallel plate geometry with a constant oscillating shear strain of 1% and angular frequency of 10 rad s⁻¹. A 50 mm parallel plate geometry with a gap size of 0.5 mm was used. The temperature was raised from 10 °C to 60 °C, at a heating rate of 1 °C min⁻¹.

Transmission electron microscopy

TEM was performed on a FEI Tecnai G2 20 TWIN with a Gatan Tridiem 863 energy filter, incorporating a built in CCD camera microscope, operating with an accelerating voltage of 200 kV. Aqueous samples of 5–25 wt% were diluted 1 : 100 and incubated at 60 °C overnight (for measurements above the LCST). The copper coated TEM grid was prepared in an oven set at 60 °C, an aliquot of the sample was placed on the grid and then negatively stained with 2% uranyl acetate. After allowing sufficient time to dry, the samples were analyzed and images were collected using a DE-16 camera.

Results and discussion

The synthesis of multi-block polymer architectures is now simplified using RDRP methods, particularly the RAFT process which is arguably the most versatile in terms of polymerization conditions, monomer functionality and monomer class.[41–43] In block copolymer synthesis, an important consideration is the order of monomer additions.

Typically, more activated monomers form the starting block, which is used as a macroRAFT agent in subsequent chain extensions with less activated monomers (LAMs), such as N-vinyl pyrrolidone (NVP), in order to minimize unwanted phenomenon such as retardation and chain termination. In this study, an unconventional block order is applied where PVP was synthesized first *via* RAFT polymerization using a R-linked difunctional xanthate RAFT agent before being chain extended with PNIPAm, a more activated monomer (MAM) (Scheme 1). There are reports of PVP-*b*-PNIPAm and PNIPAm-

b-PVP-*b*-PNIPAm being successfully synthesized *via* this approach, suggesting that the PVP R-group is an efficient leaving group and reinitiating radical for the RAFT polymerization of NIPAm.[9,16,17] In addition to block order considerations, one must also select a RAFT agent capable of controlling the polymerization of both NVP and NIPAm; something which can be accomplished with universal/switchable type RAFT agents. For example, switchable RAFT agents based on N-(4-pyridinyl)-N-methyldithiocarbamates, are effective for the synthesis of MAM-*b*-LAM type copolymers and have been used for the synthesis of well-defined poly(N,N-dimethyl-acrylamide)-*b*-poly(N-vinylpyrrolidone) (PDMAm-*b*-PVP) (Đ = 1.19).[44] The N-(4-pyridinyl)-N-methoxyphenyl dithiocarbamate showed good control over the RAFT mediated polymerization of NVP and was successfully employed for the synthesis of PNIPAM-*b*-PVP (Đ = 1.15), in organic media, with a PNIPAm macro-CTA being synthesized first.[45] There are examples, however, of well-defined poly(acrylamides) being synthesized using xanthates, hence our decision to use a xanthate for the synthesis of the tBCP, PNIPAm-*b*-PVP-*b*-PNIPAm.[46,47] Moreover, the synthesis of xanthate RAFT agents is extremely facile, which makes their use very appealing in this case. The R-linked structure of the xanthate allows for a symmetrical product in terms of chain length and chemical composition, while also having the advantage of not being readily susceptible to hydrolytic or nucleophilic cleavage.[42,43,48]

Synthesis and characterization of PVP

The descriptions of the PVP and PNIPAm-*b*-PVP-*b*-PNIPAm polymers synthesized in this study are summarized in Tables 1, 2, S1 and S2.† All RAFT polymerizations were conducted in a fully aqueous medium using the redox initiating pair, tBuOOH/Na₂SO₃. The RAFT mediated polymerization of NVP, (Scheme 1) yielded adequately well-defined PVP (Table 1), as expected with xanthate CTAs under mild aqueous conditions.[39] A mostly linear evolution of M_n with NVP conversion was observed with a continuous decrease in molecular weight dispersity throughout the polymerization, indicative of a well-controlled RAFT polymerization with fast consumption of the xanthate (Fig. S1†). Some disparities were observed between M_n^{theo}, M_n^{SEC} and M_n^{NMR}, and were ascribed to the difference in hydrodynamic volume of PVP compared to PMMA calibration standards used in SEC, and the difficulty in using quantitative end group analysis on high M_n polymers, respectively.

There was also evidence of Z-group elimination (Fig. S2 and S3†), *via* both hydrolysis and thermolysis side reactions, which can occur during polymerization, polymer work-up and storage, resulting in ω-OH and ω-unsaturated chain-ends. PVP-xanthate Z end-groups are known to be hydrolytically and thermally labile.[38,49] Nonetheless, low Đ values (≤1.3, Table 1) were obtained and Z end-group retention (Fig. S2 and S3†) was deemed adequate to proceed with towards block copolymerization.

Synthesis and characterization of PNIPAm-*b*-PVP-*b*-PNIPAm

Chain extensions with NIPAm were conducted on PVP homopolymers targeting two series of tBCPs, using PVP₁₆₀ and

PVP_{100} as macro-RAFT agents for tBCP series 1 (tBCP1) and tBCP series 2 (tBCP2), respectively. To study the effect of copolymer composition and molecular weight on the thermoresponsive properties, the permanently hydrophilic PVP segment of each tBCP series was kept constant whilst the molecular weights of the thermoresponsive PNIPAm segment were varied such that different hydrophilic fractions (f_{PVP}) were achieved. Chain extension was carried out in aqueous solutions, at a concentration of 15 wt%, initially at 50 °C under conditions analogous to those used in polymerization induced thermal self-assembly (PITSA),[50] and subsequently at 30 °C as well. PITSA, is a variant of PISA – a dispersion polymerization technique in which a solvophilic macro-RAFT agent is chain extended with a second block which is insoluble in the polymerization medium, producing self-assembled morphologies *in situ*.[51–53] Although the NIPAm monomer is soluble in aqueous solutions at elevated temperatures,[54–56] upon reaching a critical degree of polymerization, PNIPAm becomes increasingly hydrophobic forcing an *in situ* rearrangement into higher ordered morphologies made up of hydrophobic PNIPAm cores and hydrophilic PVP coronas. This is observed as a change from a transparent solution to an opaque dispersion, indicative of the coil-to-globule transition of PNIPAm.

The PVP-xanthate ω-end group is hydrolytically unstable in aqueous solutions above 40 °C,[49,57] whilst PNIPAm xanthate ω-end groups are stable under the same conditions. Therefore, we anticipated that initiating block copolymer synthesis at 50 °C could result in appreciable PVP-xanthate end group losses, negatively impacting block copolymer synthesis. This was proven *via* the chain extension performed by directly initiating the polymerization at 50 °C (entry 1, Table S2†), resulting in the formation of a poorly defined polymer which displayed significant multimodality and a broad Đ (Fig. S4, S5 and S7†). A significant proportion of PVP was not incorporated into a block copolymer, presumably because of xanthate end-group loss due to hydrolysis and/or thermolysis. To mitigate this, we adopted a protocol whereby the chain extension was initiated and maintained at 25 °C for the first 5–10 minutes, to ensure insertion of NIPAm repeat units and hence stable PNIPAm xanthate ω-end groups, before raising the reaction temperature to 50 °C until completion (entry 2, Table S2†). A chain extension performed with PVP_{242} resulted in quantitative NIPAm conversion, with SEC traces shifting to lower elution volumes, indicative of successful PNIPAm-*b*-PVP-*b*-PNIPAm synthesis. However, we also observed a shoulder on the RI trace, which did not have a matching UV-Vis signal, likely due to dead polymer chains from the first block synthesis since the shoulder was consistent with first block, based on a deconvolution of the SEC traces (Fig. S4 and S5†).

We also performed chain extensions initiated and maintained at 30 °C during the entire polymerization and obtained SEC data comparable to the system initiated at ambient temperature and ran at 50 °C (entry 3, Table S2 and Fig. S4 and S5†). Interestingly, despite the polymerization reactor being immersed into an oil bath thermostated at 30 °C, which is

below PNIPAm's LCST, the reaction mixture appeared to form a milky dispersion, consistent with PISA/PITSA systems. Presumably the reaction temperature rises above PNIPAm's LCST due to the exothermic character of the polymerization reaction, resulting in a PITSA-like system.

The polymerizations were rapid, reaching a full conversion in 2 min with reasonably low Đ, (1.32, entry 4, Table S2, Fig. S9†). We observed the presence of a small amount of dead PVP (~20%), likely present in the starting block since the trace of the block copolymer cleanly shifted to lower elution volumes. We were able to lower the Đ by increasing the [RAFT agent] : [redox initiator] ratio, to lower the radical flux hence improving control. The polymerization was still rapid, reaching full conversions in 30 minutes, and the final tBCP had a Đ of 1.30, whilst the amount of dead PVP starting blocks was estimated at 15% (entry 5 – Table S2 and Fig. S10†). The lower extent of dead PVP observed with this experiment also suggests that the higher extent of dead PVP chains observed earlier (entry 4, Table S2†) likely formed at initiation of chain extension due to a higher radical flux used then. Nevertheless, we could conclude that chain extension was successful and the amount of dead PVP starting blocks could be kept at a minimum by keeping the radical flux low and performing the polymerization at ambient temperature.

Two different series of PNIPAm-*b*-PVP-*b*-PNIPAm were synthesized, namely tBCP1 (using the PVP_{160} macro-CTA) and tBCP2 (using the PVP_{100} macro-CTA), to assess the effect of copolymer composition and molecular weight on the triblock copolymer's thermoresponsive properties. The permanently hydrophilic PVP segment of each tBCP series was kept constant with molecular weight variation of the thermoresponsive PNIPAm segment, such that different hydrophilic fractions (f_{PVP}) were achieved. The block copolymers were characterised *via* SEC, ^{1}H NMR and DOSY NMR spectroscopy. SEC analyses revealed monomodal molecular weight distributions (Đ < 1.4) with slight tailing of low molecular weight polymer, potentially corresponding to dead PVP chains, although the molecular weight distribution shift is not large enough to determine this conclusively (Fig. S11†). Block ratios were evaluated based on the ^{1}H NMR data *via* integration of backbone protons **f′** and **e** (Fig. 2, Table 2), characteristic of PNIPAm and PVP respectively. DOSY NMR analysis, Fig. 1, provided further evidence of successful chain extension as the protons corresponding to PVP and PNIPAm had similar diffusion coefficients, indicating an efficient chain extension of the PVP macro-CTA with PNIPAm.[38,58,59]

Aqueous solution properties

The temperature sensitivity of aqueous tBCP solutions was investigated using turbidimetry, *via* measurement of the optical transparency at 500 nm, with the cloud point temperature (T_{CP}) being determined as the inflection point of the transmittance curve (Fig. 3A and B). Each tBCP series was designed to have constant hydrophilic block lengths (*i.e.*, PVP_{160} for tBCP1 and PVP_{100} for tBCP2) and varying thermoresponsive PNIPAm block lengths. Both families have match-
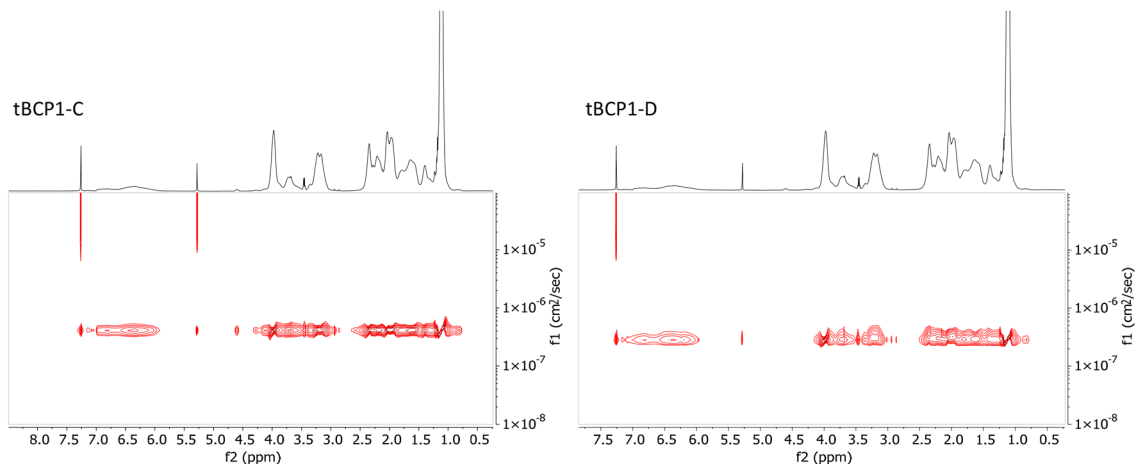
Fig. 1 DOSY NMR spectra of tBCP1-C and tBCP1-D in CDCl$_3$, both triblock copolymers showed single diffusion coefficients corresponding to 4.1×10^{-7} cm^2 s^{-1} and 3.1×10^{-7} cm^2 s^{-1}, respectively.

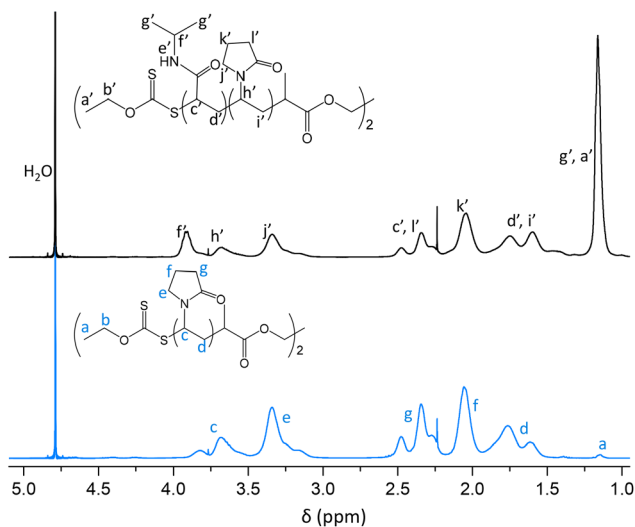**Fig. 2** Representative ^{1}H NMR spectrum of PVP$_{179}$ macro-CTA (bottom) and PNIPAm$_{234}$-b-PVP$_{179}$-b-PNIPAm$_{234}$ triblock copolymer (top) in D$_2$O.

ing overall PVP : PNIPAm ratios throughout the series. BAB type tBCPs with permanently hydrophilic middle blocks and thermoresponsive outer blocks, self-assemble into flower like micelles in dilute aqueous solutions above the LCST of the outer blocks.[11,29]

In both tBCP families, an initial sharp decrease and a subsequent gradual decrease in transmittance was observed. The initial sharp decrease became increasingly sharper with increasing PNIPAm content, and the corresponding T_{CP} decreased with increasing PNIPAm/PVP ratio (*i.e.*, decreasing hydrophilic fraction and increasing hydrophobic fraction with $T_{CP} \sim 32$ °C).[18] The sharp decrease in transmittance corresponds with the formation of flower-like micelles due to the desolvation of PNIPAm segments, while the subsequent gradual decrease in transmittance can be ascribed to the shrinkage of micelle cores with increasing temperatures, con-

sistent with observations in literature.[11] The shrinkage of micelles would generally not cause an increase in light scattering, but if there is some hydrophilic bridging between micelles present, which becomes increasingly more likely with increasing molecular weight and tBCP concentration, then shrinkage of micelle PNIPAm cores would effectively create larger tightly packed agglomerates of linked micelles which scatter greater amounts of light, thereby decreasing the transmittance. For a given hydrophilic fraction, tBCP1 with a larger molecular weight displayed a greater change in transmittance compared to corresponding tBCP2 analogues, as it is likely that the polymers of lower molecular weight and lower PNIPAm composition might not create a network of flower-like micelles (*i.e.* gel) but rather just dispersed micelles in solution which scatter light to a lesser extent. The T_{CP} values of tBCP2 were higher compared to tBCP1 throughout the series, as this series comprises lower molecular weight polymers, per PNIPAm/PVP composition, which are comparatively more stable against desolvation than higher molecular weight chains (Fig. 3C). The inverse relationship between molecular weight and the T_{CP} value for thermoresponsive polymers has been previously reported.[13,16,60]

The thermo-induced phase transition for dilute aqueous solutions of the tBCP1 series was investigated *via* a variable temperature DLS analysis (Fig. 3, S12–S14†). Size distributions were obtained every 2 °C between 20–50 °C where a monomodal population corresponding to tBCP1-A, tBCP1-C and tBCP1-D unimers with hydrodynamic diameters (D_h) of approximately 8, 11 and 13 nm respectively, was observed. At an onset temperature of 42, 36 and 34 °C for tBCP1-A, C and D, respectively, a sharp increase in D_h was observed due to dehydration of the hydrophobic PNIPAm blocks and the resultant agglomeration of several tBCP unimers into flower-like micelles. The inflection point for the increase in D_h was determined to be 43, 37 and 35 °C for tBCP1-A, C and D respectively which agreed relatively well to the T_{CP} values obtained for these samples (44, 39 and 37 °C respectively). tBCP1-A has the lowest PNIPAm frac-
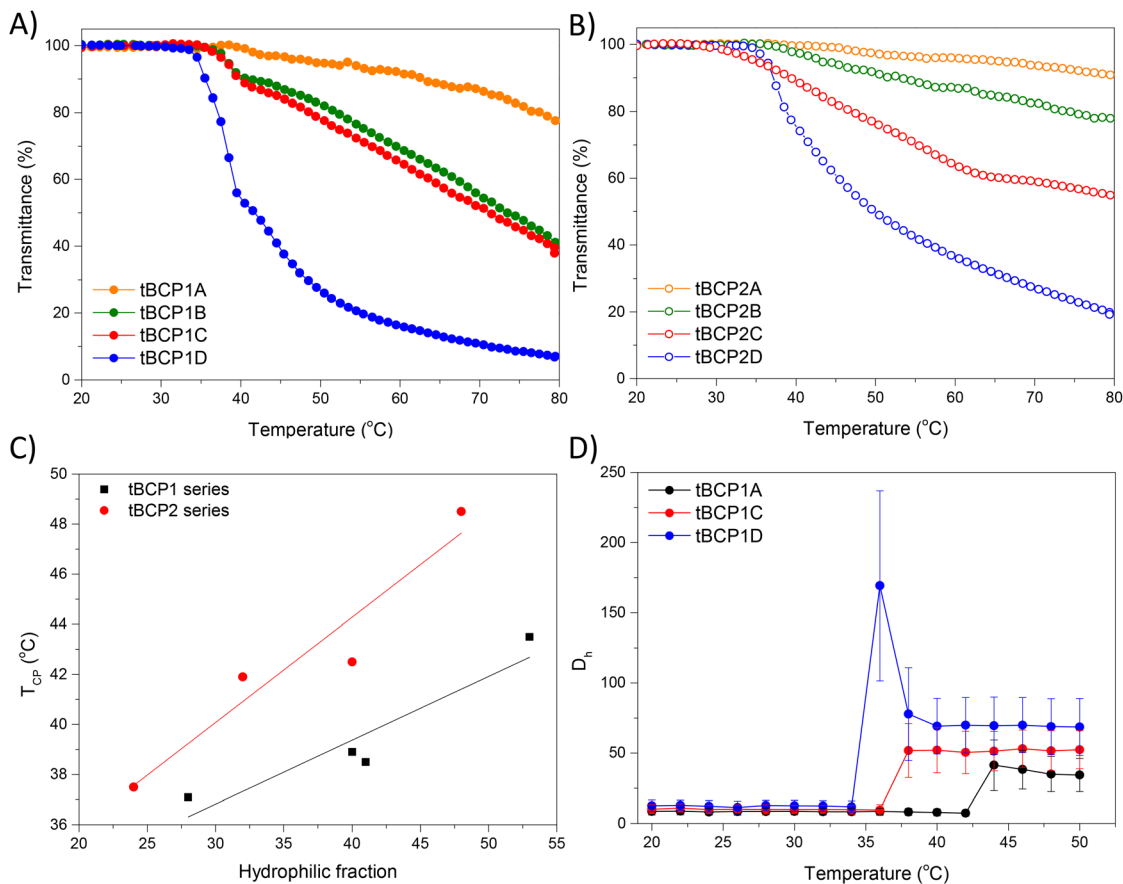
Fig. 3 Turbidity curves and relationship between hydrophilic fraction and cloud point temperature of 10 wt% tBCP1 (A), tBCP2 (B), and T_{CP} values (C) as a function of the tBCP hydrophilic fraction; T_{CP} was selected as the temperature at which the transmittance data exhibited an inflection point (determined using the first derivative of the curve). The change in hydrodynamic diameter as a function of temperature was determined *via* DLS (D) for tBCP1-A, tBCP1-C and tBCP1-D (all at 1 mg mL^{-1}).

tion of the three tBCPs analysed and thus its unimers are effectively solubilized by the permanently hydrophilic PVP segments up to much higher temperatures compared to tBCP1-C and tBCP1-D which have increasing PNIPAM block lengths. Once the rapid desolvation of PNIPAm occurs in tBCP1-A, micelles of approximately 34 nm are obtained, whereas the tBCP1-C micelles with higher PNIPAm content are slightly larger at ~51 nm. This increase in size could be a result of the larger PNIPAm segments, which constitute the core of the micelles, compared to tBCP1-A. This potentially requires a larger number of unimers to stabilize the more hydrophobic tBCP in aqueous solution once the PNIPAm segments have transitioned from random coils to collapsed chains.

tBCP1-D displayed a slightly different response to the gradual increase in temperature, as after the sharp increase at 34 °C, a steep decrease in D_h was observed after which the micelles stabilized at ~70 nm. The lower PVP fraction of this tBCP results in decreased solubilizing efficiency of the PVP segments at increasingly higher temperatures, so not only is micelle formation being observed but also the continued dehydration and shrinkage of the PNIPAm core.[24,61]

TEM analysis of tBCP1-C and tBCP-1D samples (Fig. 4), prepared from a 0.15 wt% aqueous solution also revealed the formation of individual spherical micelles, without any extensive agglomeration, confirming that the aggregates observed *via* DLS are micelles, presumably flower like, as expected for BAB type tBCPs.
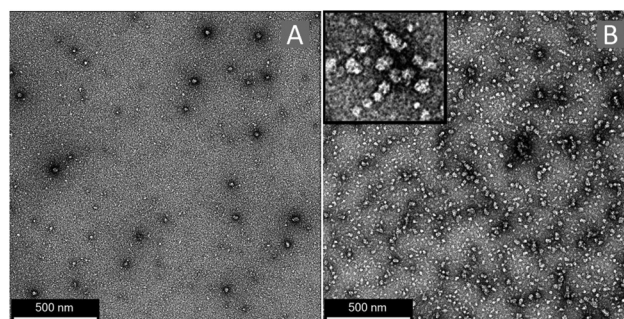

Fig. 4 TEM images of 0.15 wt% tBCP1-C (A) and tBCP1-D (B) at 60 °C (negatively stained with 2% uranyl acetate).

The influence of tBCP concentration on thermoresponsivity was also investigated *via* turbidimetry, using tBCP1-D with concentrations from 5 to 25 wt%, where a decrease in T_{CP} values was observed with increasing tBCP concentration (Fig. 5 and S15†). Increasing concentrations are known to reduce T_{CP} values due to the shorter distance among polymer chains resulting in a higher probability of aggregation amongst hydrophobic domains.[60] A two-step transition was also observed with an initial steep drop in transmittance followed by a gradual decrease in transmittance. At tBCP1-D concentrations below the critical gelation concentration, an increase in temperature above the LCST results in the desolvation of the PNIPAm segments and formation of disperse flower-like micelles. Above the CGC, polymer chains are in closer proximity and there is a higher probability of chains being associated with more than one micelle, where the hydrophilic PVP segments are the bridging components. If there are enough interpenetrating chains and associated micelles, a gel is obtained. The temperature at which this occurs decreases with increasing tBCP concentration as the effective concentration of PNIPAm that undergoes desolvation increases.

To gain more understanding of the thermo-induced phase transition of the tBCPs in aqueous solutions, we conducted variable temperature ^{1}H NMR spectroscopic analysis of tBCP-1D in D$_2$O (Fig. S16†). Temperature-induced association of the block copolymers can be observed once the transition temperature is reached due to the 'disappearance' of characteristic peaks of hydrophobic components of the tBCP.[6,17] The intensities of signals corresponding to PNIPAm's methine and methyl backbone protons decreased drastically from 40 °C and almost entirely disappear with further increase in temperature, due to desolvation and reduced mobility of PNIPAm block segments.[17] The hydrophilic PVP's signals remained well resolved. This is an indication of self-assembly taking place with increasing temperature, with the hydrophilic PVP segments shielding the desolvated PNIPAm segments. The normalized

NMR peak intensity ratios of PNIPAm : PVP (I1.2/I3.3) were calculated for each temperature increment and plotted as a function of temperature, as indicated in Fig. S16.†

Formation of hydrogels *via* thermo-induced sol–gel transition

The ability of the tBCPs to display a thermo-induced sol–gel transition was first screened *via* the vial-inversion method. Aqueous tBCP solutions of concentrations ranging from 5 to 25 wt% were heated to 60 °C in an oil bath before removing the sample from the bath and inverting the sample vial. The samples were classified as hydrogels if they were able to support their own weight for at least 1 minute. The samples tBCP1-A and tBCP2-A & B, were incapable of gelation up to 25 wt%. It is likely that this is caused by a combination of the relatively low overall DP of these tBCPs and the concentrations used. Thermo-induced sol–gel transitions have been observed with ABA type tBCPS with comparable molecular weights based on PNIPAm or poly(di(ethylene glycol)ethyl ether acrylate) thermoresponsive A-blocks and poly(N,N-dimethylacrylamide) hydrophilic B-blocks, at 50 wt%.[55] Hydrogels were obtained at a critical gelation concentration (CGC) of 25 wt% for tBCP2-C, 20 wt% for tBCP1-C and tBCP2-D, and 15 wt% for tBCP1-D.

The apparent CGCs decreased as the tBCPs molecular weight increased (tBCP2-C and tBCP1-C) as expected since higher molecular weight tBCPs are effective gelators at lower concentrations. The tBCPs 1-C and 2-D with respective compositions of PNIPAm$_{120}$-*b*-PVP$_{160}$-*b*-PNIPAm$_{120}$ and PNIPAm$_{180}$-*b*-PVP$_{100}$-*b*-PNIPAm$_{180}$ and respective M_n values of 45 000 g mol^{-1} and 53 000 g mol^{-1}, both display a CGC of 20 wt%. The length of the hydrophilic bridging blocks is known to dictate the CGC, whilst the thermoresponsive hydrophobic blocks help to enhance the mechanical strength of the gels.[62] The tBCP1-D with both the largest molar mass and hydrophilic block length in this study gave the lowest CGC as expected. Reversibility of the thermo-induced sol–gel transition was confirmed by cooling the samples as depicted in Fig. 6A.

To gain a more objective perspective of the thermo-induced sol–gel transitions, we investigated this behavior *via* variable temperature rheology, to evaluate the effect of temperature on the loss modulus (G') and the storage modulus (G'') (Fig. 6B). We used aqueous solutions of tBCP-1C, 1D and 2D at a sample concentration of 25 wt%. The gelation temperature (T_{gel}) was determined as the point where the storage modulus (G') exceeds the loss modulus (G''). As shown in Fig. 6B, this analysis also revealed a two-step transition in the variation of G' and G'' with increasing temperature for all the samples tested, consistent with observations in the turbidimetry studies and DLS studies. At low temperatures, G' was lower than G'', indicating that the solutions were free-flowing liquids.

An initial thickening, indicative of a viscous liquid, was observed at ~30 °C for tBCP1-C and tBCP2-D and at ~28 °C for tBCP1-D when both G' and G'' started to increase, but with G' still less than G''. Crossover points where G' exceeds G'' were observed at 36.9, 32.3 and 37.6 °C for tBCP1-C, tBCP1-D and tBCP2-D, respectively, indicating the gel point temperatures
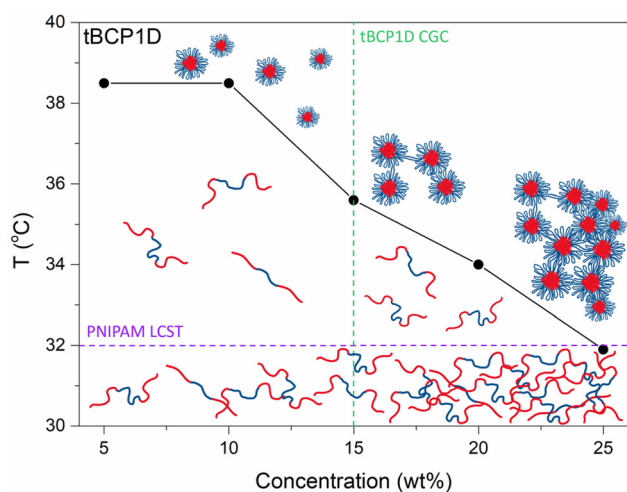

Fig. 5 The effect of concentration of tBCP1-D on the cloud point temperature.
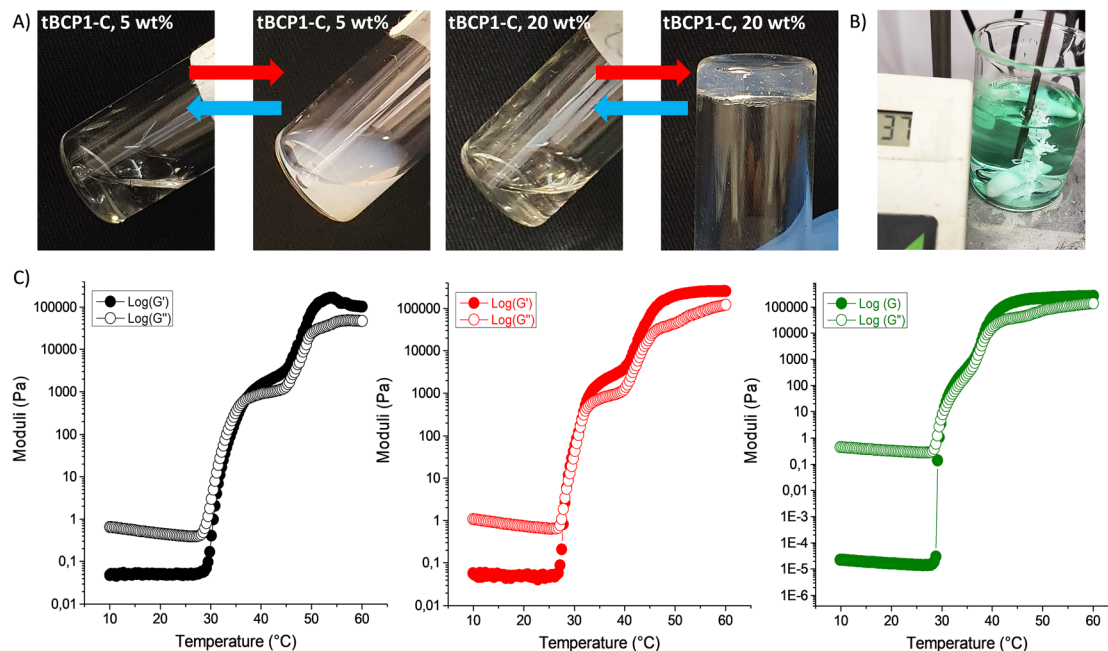
Fig. 6 (A) Typical images showing aqueous solutions of tBCP1-C at low concentration (5 wt%, left) and high concentration (20 wt%, right). (B) Solution of PNIPAM$_{234}$-b-PVP$_{179}$-b-PNIPAM$_{234}$ tBCP at 10 wt% injected into 37 °C water *via* a 22-gauge needle. The gel remained intact after 3 h of stirring at 37 °C, with complete exclusion of the hydrophilic dye from the hydrophobic confines of the gel. (C) Rheology of tBCP-1C (black), tBCP1-D (red) and tBCP2-D (green) where G' is indicated as closed symbols and G'' as open symbols.

for the respective tBCPs, as seen *via* variable temperature rheology. Thereafter, the increase of both G' and G'' with temperature slows down, and both appear to plateau, before increasing sharply again, still with $G' > G''$, and levelling at almost two orders of magnitude the G' and G'' values for the first step. Two-step sol–gel transitions have been observed with a PNIPAm-b-PDMam-b-PNIPAm tBCP in water, in which the solution viscosity initially increased, with $G' < G''$, before the crossover was observed.[12] For BAB triblock copolymers, with a permanently hydrophilic A block and thermoresponsive B block, a transition from Newtonian fluid to flower-like micelles occurs upon reaching the T_{CP}. With further increase in temperature, when the tBCP concentration is high enough such that intermicellar distances are short, hydrophilic bridges between the micelles start forming, forming a three-dimensional network, as reflected by G' becoming greater than G''.

This is forced by unfavourable enthalpic interactions between dangling chain ends and an unfavourable solvent. The extent of bridging is dependent on the degree of hydration as well as the block lengths and ratios, hence the apparent dependence of the sol–gel transition on tBCP composition. As temperature increases further, more bridging occurs resulting in a stronger network; this likely explains the observation of a two-step transition.[29]

The injectability of the PNIPAM$_{234}$-b-PVP$_{179}$-b-PNIPAM$_{234}$ tBCP (Table S2,† entry 5) was investigated, whereby a 10 wt% solution of the tBCP was prepared, colored with green hydrophilic dye, and injected into water heated to 37 °C *via* a 22 gauge (0.70 × 30 mm) needle. Upon injection (Movie S1,

ESI†), a rapid sol–gel transition was observed resulting in a thin strand of PNIPAM$_{234}$-b-PVP$_{179}$-b-PNIPAM$_{234}$ gel which did not dissolve upon continued stirring at 37 °C. This demonstrates the potential of these tBCPs as injectable hydrogels.

Conclusions

In conclusion, we have shown a facile synthesis of well-defined thermoresponsive triblock copolymer based on PNIPAm-b-PVP-b-PNIPAm *via* xanthate mediated RAFT polymerization, in water – potentially advantageous for biomedical applications requiring use of thermoresponsive polymeric hydrogels. PVP was used as our starting hydrophilic block, before chain extension with PNIPAm to obtain well-defined PNIPAm-b-PVP-b-PNIPAm, as indicated by ^{1}H NMR, 2D DOSY NMR and SEC analyses.

We studied the temperature induced self-assembly using a combination of techniques, including turbidimetric analysis, DLS, ^{1}H NMR spectroscopy and TEM. The cloud point temperature (T_{CP}) was dependent on the copolymer composition, concentration, and molecular weight of the tBCP. The tBCPs self-assemble into uniform flower-like micelles, which contract with increasing temperature, likely due to shrinkage of the micelle core with increasing temperature. This manifests in the form of a two-step transition in the turbidimetric analysis and decrease in micelle sizes in DLS analysis. Concentrated aqueous solutions of the tBCPs form free-standing thermoreversible hydrogels, as shown by test-tube inversion tests and

variable temperature rheological experiments. The appeal of this system is the facile synthesis, in water, without recourse to tedious post-polymerization functionalisation steps in organic solvents. This should increase the appeal of these PNIPAm-*b*-PVP-*b*-PNIPAm as stimuli responsive hydrogels for biomedical applications.

Conflicts of interest

There are no conflicts to declare.

Acknowledgements

References

1 M. Mahinroosta, Z. Jomeh, A. Allahverdi and Z. Shakoori, *Mater. Today Chem.*, 2018, **8**, 42–55.

2 K. Varaprasad, G. Malegowd, T. Jayaramudu, M. Mohan and R. Sadiku, *Mater. Sci. Eng., C*, 2017, **79**, 958–971.

3 D. A. Gyles, L. D. Castro, J. O. C. Silva and R. M. Ribeiro-Costa, *Eur. Polym. J.*, 2017, **88**, 373–392.

4 A. S. Hoffman, *Adv. Drug Delivery Rev.*, 2012, **64**, 18–23.

5 T. Thambi, Y. Li and D. S. Lee, *J. Controlled Release*, 2017, **267**, 57–66.

6 J. Giliomee, R. Pfukwa, N. P. Gule and B. Klumperman, *Polym. Chem.*, 2016, **7**, 1138–1146.

7 M. C. Koetting, J. T. Peters, S. D. Steichen and N. A. Peppas, *Mater. Sci. Eng., R*, 2015, **93**, 1–49.

8 D. M. Devine and C. L. Higginbotham, *Polymer*, 2003, **44**, 7851–7860.

9 Z. Zhu and S. A. Sukhishvili, *ACS Nano*, 2009, **3**, 3595–3605.

10 T. J. Smith, J. E. Kennedy and C. L. Higginbotham, *J. Mater. Sci.*, 2010, **45**, 2884–2891.

11 A. Zahoranová, M. Mrlík, K. Tomanová, J. Kronek and R. Luxenhofer, *Macromol. Chem. Phys.*, 2017, **218**, 1–12.

12 L. Despax, J. Fitremann, M. Destarac and S. Harrisson, *Polym. Chem.*, 2016, **7**, 3375–3377.

13 S. Cui, L. Yu and J. Ding, *Macromolecules*, 2019, **52**, 3697–3715.

14 T. G. O'Lenick, X. Jiang and B. Zhao, *Langmuir*, 2010, **26**, 8787–8796.

15 Y. J. Kim and Y. T. Matsunaga, *J. Mater. Chem. B*, 2017, **5**, 4307–4321.

16 H. Cong, J. Li, L. Li and S. Zheng, *Eur. Polym. J.*, 2014, **61**, 23–32.

17 S. I. Yusa, S. Yamago, M. Sugahara, S. Morikawa, T. Yamamoto and Y. Morishima, *Macromolecules*, 2007, **40**, 5907–5915.

18 A. Halperin, M. Kröger and F. M. Winnik, *Angew. Chem., Int. Ed.*, 2015, **54**, 15342–15367.

19 Y. Zeng and W. G. Pitt, *J. Biomater. Sci., Polym. Ed.*, 2005, **16**, 371–380.

20 M. Sahn, T. Yildirim, M. Dirauf, C. Weber, P. Sungur, S. Hoeppener and U. S. Schubert, *Macromolecules*, 2016, **49**, 7257–7267.

21 Y. Zhou, K. Jiang, Q. Song and S. Liu, *Langmuir*, 2007, **23**, 13076–13084.

22 C. Zhou, Y. Chen, M. Huang, Y. Ling, L. Yang, G. Zhao and J. Chen, *New J. Chem.*, 2021, **45**, 5925–5932.

23 Y. Chen, Y. Gao, L. P. da Silva, R. P. Pirraco, M. Ma, L. Yang, R. L. Reis and J. Chen, *Polym. Chem.*, 2018, **9**, 4063–4072.

24 Y. Li, Z. Ye, L. Shen, Y. Xu, A. Zhu, P. Wu and Z. An, *Macromolecules*, 2016, **49**, 3038–3048.

25 W. Wang, C. Gao, Y. Qu, Z. Song and W. Zhang, *Macromolecules*, 2016, **49**, 2772–2781.

26 S. Sistach, M. Beija, V. Rahal, A. Brûlet, J. D. Marty, M. Destarac and C. Mingotaud, *Chem. Mater.*, 2010, **22**, 3712–3724.

27 C. A. Figg, A. Simula, K. A. Gebre, B. S. Tucker, D. M. Haddleton and B. S. Sumerlin, *Chem. Sci.*, 2015, **6**, 1230–1236.

28 T. M. Legge, A. T. Slark and S. Perrier, *Macromolecules*, 2007, **40**, 2318–2326.

29 B. D. Monnery and R. Hoogenboom, *Polym. Chem.*, 2019, **10**, 3480–3487.

30 C. T. Huynh, M. K. Nguyen and D. S. Lee, *Macromolecules*, 2011, **44**, 6629–6636.

31 A. Guinaudeau, S. Ephane Mazi Eres, D. J. Wilson and M. Destarac, *Polym. Chem.*, 2012, **3**, 33.

32 R. Devasia, R. L. Bindu, R. Borsali, N. Mougin and Y. Gnanou, *Macromol. Symp.*, 2005, **229**, 8–17.

33 O. J. Deane, J. R. Lovett, O. M. Musa, A. Fernyhough and S. P. Armes, *Macromolecules*, 2018, **51**, 7756–7766.

34 N. Bailly, M. Thomas and B. Klumperman, *Biomacromolecules*, 2012, **13**, 4109–4117.

35 M. Teodorescu and M. Bercea, *Polym.-Plast. Technol. Eng.*, 2015, **54**(9), 923–943.

36 M. K. Chun, C. S. Cho and H. K. Choi, *J. Appl. Polym. Sci.*, 2004, **94**(6), 2390–2394.

37 E. J. P. Jansen, R. E. J. Sladek, H. Bahar, A. Yaffe, M. J. Gijbels, R. Kuijer, S. K. Bulstra, N. A. Guldemond and I. Binderman, *Biomaterials*, 2005, **26**(21), 4423–4431.

38 A. Guinaudeau, O. Coutelier, A. Sandeau, S. Mazières, H. D. Nguyen Thi, V. Le Drogo, D. J. Wilson and M. Destarac, *Macromolecules*, 2014, **47**, 41–50.

39 A. J. Convertine, B. S. Lokitz, Y. Vasileva, L. J. Myrick, C. W. Scales, A. B. Lowe and C. L. McCormick, *Macromolecules*, 2006, **39**(5), 1724–1730.

40 D. Taton, A. Z. Wilczewska and M. Destarac, *Macromol. Rapid Commun.*, 2001, **22**, 1497–1503.

41 D. J. Keddie, G. Moad, E. Rizzardo and S. H. Thang, *Macromolecules*, 2012, **45**, 5321–5342.

42 G. Moad, *Polym. Chem.*, 2017, **8**, 177–219.

43 D. J. Keddie, *Chem. Soc. Rev.*, 2014, **43**, 496–505.

44 D. J. Keddie, C. Guerrero-Sanchez, G. Moad, E. Rizzardo and S. H. Thang, *Macromolecules*, 2011, **44**, 6738–6745.

45 S. J. Stace, G. Moad, C. M. Fellows and D. J. Keddie, *Polym. Chem.*, 2015, **6**, 7119–7126.

46 E. Read, A. Guinaudeau, D. J. Wilson, A. Cadix, F. Violleau and M. Destarac, *Polym. Chem.*, 2014, **5**, 2202–2207.

47 A. Glaria, M. Beija, R. Bordes, M. Destarac and J. D. Marty, *Chem. Mater.*, 2013, **25**, 1868–1876.

48 G. Moad, E. Rizzardo and S. H. Thang, *Aust. J. Chem.*, 2005, **58**, 379–410.

49 G. Pound, J. M. McKenzie, R. F. M. Lange and B. Klumperman, *Chem. Commun.*, 2008, **27**, 3193–3195.

50 C. A. Figg, A. Simula, K. A. Gebre, B. S. Tucker, D. M. Haddleton and B. S. Sumerlin, *Chem. Sci.*, 2015, **6**, 1230–1236.

51 S. L. Canning, G. N. Smith and S. P. Armes, *Macromolecules*, 2016, **49**, 1985–2001.

52 C. Liu, C. Y. Hong and C. Y. Pan, *Polym. Chem.*, 2020, **11**, 3673–3689.

53 X. Wang, S. Li, Y. Su, F. Huo and W. Zhang, *J. Polym. Sci., Part A: Polym. Chem.*, 2013, **51**, 2188–2198.

54 R. Francis, K. B. Deepa and S. Kumar, *J. Appl. Polym. Sci.*, 2012, **124**, 5079–5088.

55 Y. Zhao, X. J. Ju, L. P. Zhang, W. Wang, Y. Faraj, L. B. Zou, R. Xie, Z. Liu and L. Y. Chu, *New J. Chem.*, 2019, **43**, 9507–9515.

56 D. Gan and L. A. Lyon, *Macromolecules*, 2002, **35**, 9634–9639.

57 S. Jharimune, R. Pfukwa, Z. Chen, J. Anderson, B. Klumperman and R. M. Rioux, *J. Am. Chem. Soc.*, 2021, **143**(1), 184–195.

58 F. Coumes, C. Y. Huang, C. H. Huang, J. Coudane, D. Domurado, S. Li, V. Darcos and M. H. Huang, *Biomacromolecules*, 2015, **16**, 3666–3673.

59 P. Groves, *Polym. Chem.*, 2017, **8**, 6700–6708.

60 X. Zhao, W. Liu, D. Chen, X. Lin and W. W. Lu, *Macromol. Chem. Phys.*, 2007, **208**, 1773–1781.

61 V. Aseyev, S. Hietala, A. Laukkanen, M. Nuopponen, O. Confortini, F. E. Du Prez and H. Tenhu, *Polymer*, 2005, **46**, 7118–7131.

62 A. P. Vogt and B. S. Sumerlin, *Soft Matter*, 2009, **5**, 2347–2351.